Morphology-Changeable Soft Pads Facilitate Locomotion in Wet Conditions

Duy Dang Nguyen, *Graduate Student Member, IEEE*, Nhan Huu Nguyen, *Member, IEEE*, and Van Anh Ho, *Senior Member, IEEE*

***Abstract*—Stable robot walking requires effective gait planning and control. The mechanical properties of contact between feet and ground are important factors in this process. In this paper, we propose a design of robot foot that houses soft pads, which adapt to facilitate locomotion on wet and dry floors. The morphology of each soft pad distributed in the foot is changed from a thin elastic sheet to a spherical dome that protrudes from the sole by using compressed air to adapt the foot for walking. We constructed an analytical model to estimate how soft pad dome is affected by air pressure and associated properties regarding friction and forces when in contact with a dry or wet floor. The contribution of wet adhesion to enhance shear force among the floor and the soft pads was elaborated theoretically. We report results of practical experiments with a sole (35 mm × 15 mm) housing 14 such soft domes (radius 1.5 mm) comparing walking in dry and wet conditions. Finally, we present a setup of a walking robot leg with the proposed foot and soft pad on flat ground. The results demonstrate that soft pad domes improved walking stability under wet conditions on flat ground whereas they made no noticeable difference under dry conditions. Changeable morphology of the domes (stiffness, radius), which is controlled by adjusting air pressure, contributed to adaptive walking. The results obtained here may inform attempts at morphological design of soft pads to facilitate locomotion of legged robots under various terrain conditions.**

***Index Terms*—Tribology, capillary, morphology computation, soft toe pad, animal locomotion.**

I. Introduction

RECENTLY, biomimetic research has been applied to develop promising functions in engineering systems [1]; and to test biological hypotheses difficult to test in living creatures [2]. This approach offers possibilities to discover underlying physics which cannot be verified ethically or systematically in animals. Of many biomimetic approaches, studies leveraging morphological adaptation to environment conditions and creating new functions that cannot be implemented in fixed morphology have been recently pursued [3].

Animal adaptation to environments based on ability to change morphology, widely referred to as the concept of morphological design, has been investigated [4]. Especially, the role of tribological phenomena of human fingers in grasping, gecko toes in dry locomotion [5], and tree frog toes in wet gripping [6] have been investigated with findings applied to engineering. Morphological adaptation and tribology in starfish, which pump water into tubular limbs through a sieve plate in the skin to alter morphology, such as shape, stiffness, and posture to facilitate locomotion has been reported [7]. Such animals adapt their morphology to exploit tribology, enabling adhesion between limbs and surfaces for locomotion in complicated environments [8]. Application of such phenomena might go some way to prevent slippage that may ordinarily occur if a legged robot walks on a wet or even a dry surface.

Here, we propose a novel design robot foot with a pad that changes its morphology to facilitate walking under dry and wet conditions. An analytical model of the designed sole was developed to examine relationships between its morphology and ground contact conditions. In addition, by actively changing the morphology of soft pads in the sole to adapt to different surface conditions, we demonstrate that morphological aspects may play important roles for legged walking robots.

II. Related Work

A. Morphology of Animal Toe Pad and Applications

Gavin et al. [9] reported that tree frog toe pads exhibit velocity-dependent resistance to shear, which has been widely applied to wet adhesion mechanisms [10]. The hierarchical structure of gecko toe pads has been extensively studied [11]; and its application in dry adhesion mechanisms has been reported [12]. It was reported that geckos change their hydrophobicity in humid environments to maximize adhesion and stabilize friction forces [13]. Adhesion by echinoderm tube feet enabling animals to traverse surfaces such as sand, stone, or underwater surfaces has been studied [14]. Starfish-inspired tube feet were designed and fabricated to demonstrate robust adhesion and locomotion [15]. A soft pad claw robot, which exploits the morphology of flexible pads, demonstrated ability to climb rough vertical

Manuscript received 17 October 2022; accepted 24 March 2023. Date of publication 5 April 2023; date of current version 12 April 2023. This letter was recommended for publication by Associate Editor E. W. Hawkes and Editor Y.-L. Park upon evaluation of the reviewers' comments. This work was supported by the Japan Society for the Promotion of Science (JSPS) Grant-in-Aid for Scientific Research KAKENHI under Grant 21H01287. *(Corresponding author: Van Anh Ho.)*

Duy Dang Nguyen and Nhan Huu Nguyen are with the Soft Haptics Lab., School of Materials Science, Japan Advanced Institute of Science and Technology, Nomi, Ishikawa 923-1292, Japan (e-mail: duy_nguyen@jaist.ac.jp; nhnhan@jaist.ac.jp).

Van Anh Ho is with the Soft Haptics Lab., School of Materials Science, Japan Advanced Institute of Science and Technology, Nomi, Ishikawa 923-1292, Japan, and also with the Japan Science and Technology Agency, PRESTO, Kawaguchi Saitama 332-0012, Japan (e-mail: van-ho@jaist.ac.jp).

This letter has supplementary downloadable material available at https://doi.org/10.1109/LRA.2023.3264731, provided by the authors.

Digital Object Identifier 10.1109/LRA.2023.3264731

This work is licensed under a Creative Commons Attribution 4.0 License. For more information, see https://creativecommons.org/licenses/by/4.0/

surfaces [16]. And a quadruped insect-scale robot used capillary and lubrication effects for inclined climbing [17].

B. Soft Contact Mechanics

Soft contact locomotion by animals and robots as mentioned above involves tribological properties including adhesion, friction, capillary action, Van de Waal force, and others. However, it is challenging to assess the role each plays in specific scenarios, especially when most pads on the feet of living creatures are soft and flexible. One approach may be to construct a capillary-action model using elastic material. Based on Hertz theory, Johnson-Kendall-Roberts [18], Derjaguin–Muller–Toporov [19], and Tabor [20] proposed explanations of various contact conditions for soft bodies. Maugis-Dugdale theory [21] provided analytical data in the intermediate regions where Tabor number has moderate values. We previously investigated soft contact by wet adhesion of a micro-patterned pad [22]; and inspired by tree frog toes, proposed a morphology for the pad to grasp a thin hemispherical shell using wet adhesion [23], [24].

The present study is a theoretical and experimental investigation of soft pads with changeable morphology to aid stable walking of a robot foot on dry and wet floors. The contributions are as follows:

- We propose the design of soft pad that can morph between a flat elastic sheet in the foot sole (for walking in dry condition) to a protruding spherical dome to enhance walking efficiency on wet surfaces.
- We propose an analytical model to investigate the soft pad morphology, and tribology including friction, adhesion, and capillary action.
- We describe practical experiments with a robot foot equipped with the aforementioned soft pads that demonstrate they facilitate walking efficiency.

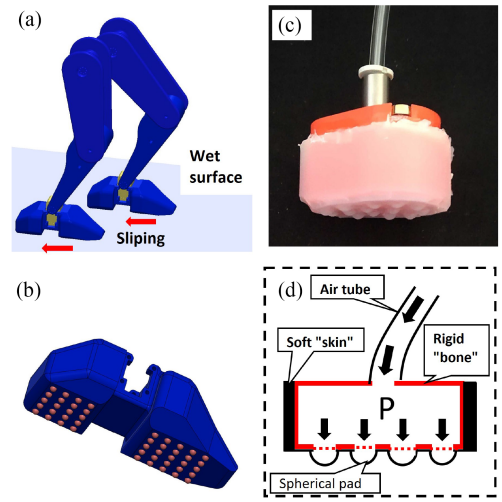

Fig. 1. Morphology-changeable soft pads for walking on both wet and dry floors. (a) Concept of a legged robot with possible slippage on a wet floor. (b) Concept of a robot foot with an adaptable sole. (c) Fabrication of a robotic foot including a rigid "bone" enveloped by soft skin, and a soft sole with adaptable soft pads. (d) Cross-sectional sketch of the foot showing adaptable soft pads controlled by pneumatic air.

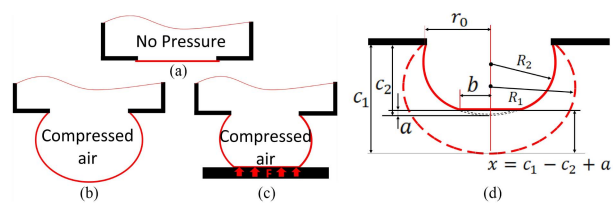

Fig. 2. States of soft pads. (a) Without air pressure (flat circular soft pad). (b) With air pressure (dome shaped soft pad) without floor contact, (c) and with floor contact upon walking. (d) Geometrical parameters (at constant pressures) of the soft pad with and without contact (dashed line).

III. Analytical Model

A. Morphology Computation Model

The conceptual design and a prototype foot with soft pads are shown in Fig. 1. Soft pads in the sole are adapted to facilitate walking on a wet floor by application of compressed air which changes their morphology from a flat sheet to a spherical dome. In this section, we present a theoretical explanation of the principles of this adaptation and resulting adhesion upon contact with a wet floor. During walking, an inflated soft pad interacts with the floor at contact force $\mathbf{F}$. First, an analytical model is discussed regarding relationships between soft pad morphology and F and p values. A soft pad in three possible states is illustrated in Fig. 2(a)–(c), without pressure (flat circular sheet), adapted by air pressure (spherical dome) without simulated floor contact, and with simulated floor contact (resultant change in morphology). The force pressing a pad onto the floor changes the pad condition from high potential equilibrium (when it assumes a spherical shape with resultant volume V_1) to a lower potential state (when contact occurs with resultant volume V_2) of a thin elastic sheet (see Fig. 2(d)). The total energy in the system including potential energy of compressed air U_p, elastic tension of thin sheet U_{te}, and adhesive energy absorbed by adhesion U_{ad} may be calculated as:

$$U_{tot} = U_p + U_{te} - U_{ad}, \tag{1}$$

where U_p can be estimated using the following expression:

$$U_p = pV_1 - pV_2. \tag{2}$$

According to the geometrical properties shown in Fig. 2(d), resultant volumes at two states of the dome can be calculated as: $V_1 = \frac{\pi}{6}c_1(3r_0^2 + c_1^2)$, and $V_2 = \frac{\pi}{6}c_2(3r_0^2 + c_2^2) - \frac{\pi}{6}a(3b^2 + a^2)$. Thus, U_p can be estimated as :

$$U_p = pV_1 - p\frac{\pi}{6}c_2\left(3r_0^2 + c_2^2\right) + p\frac{\pi}{6}a\left(3b^2 + a^2\right). \tag{3}$$

Next, tension energy U_{te} at the spherical dome surface may be considered as potential strain energy of an elastic sheet under constraint. The model proposed by [25] to represent inflation of an elastic balloon is not applicable for part of the pad (i.e., spherical dome shape) with related constraints. Here, we propose a definition of tension energy as the elastic energy of the thin sheet stretched in all directions (see Fig. 3).

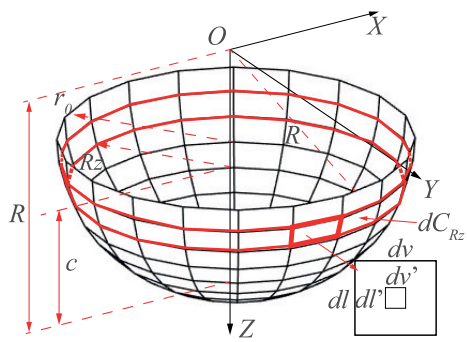

Fig. 3. Differential of spherical surface of foot pad as explanation of tension energy: tension energy is calculated from the integrals of differentials of spherical segments along the z-axis.

Considering an infinitesimal area $dv'dl'$ on the sheet surface at height $(R-c)$ along Z-axis of the coordinates $O-XYZ$, and on the region (red-colored band) with radius R_z. Let us assume that under low air pressure, the area is stretched to $dvdl$ at the same height (or value of R_z unchanged); therefore, the necessary work to this stretching can be limited to those of XY-axes as shown below:

$$dW_{te} = dW_x + dW_y = \frac{1}{2}Tdu_xdu_y + \frac{1}{2}Tdu_ydu_x, \tag{4}$$

where T is the elastic tension of the thin sheet. Given uniform deformation of the thin sheet at all points and directions, elongation along XY-axes can be estimated as follows:

$$du_x = du_y = d(l-l') = d(v-v') = dl = dv. \tag{5}$$

Considering the deformation of the sphere, we divide the sphere into segments which called dC_{R_z}. Thus, the tension potential is integral to the work for deformation of the soft pad segment following z-axis:

$$dW_{te} = Tdldv, dW_{r_z} = \int_{dC_{R_z}} dW_{te} = TdC_{R_z} \tag{6}$$

$$\longrightarrow W_{te} = \int_Z TdC_{R_z} = \pi T(r_0^2 + c^2). \tag{7}$$

We consider the tension T when the soft pad inflates

$$dl = du + dl,' \text{ and } dv = du + dv'.$$

The elastic tension that is considered for each element of differential of sphere area:

$$T = k\frac{du}{dl'} = k\frac{du}{dv'}$$
$$\rightarrow T = k\left(\frac{dl}{dl'} - 1\right) = k\left(\frac{dv}{dv'} - 1\right), \tag{8}$$

$$\longrightarrow \left(\frac{T}{k} + 1\right)^2 = \frac{dldv}{dl'dv'} = \frac{dS}{dS'} \rightarrow T = k\frac{\sqrt{S} - \sqrt{S'}}{\sqrt{S'}}. \tag{9}$$

This result leads to the potential energy for state 1 of a spherical soft pad as below:

$$\longrightarrow W_{te} = \pi k\frac{\sqrt{r_0^2 + c_1^2} - r_0}{r_0}(r_0^2 + c_1^2). \tag{10}$$

Besides, the potential energy for state 2 of the spherical soft pad is built based on geometrical parameters in this case:

$$\longrightarrow W_{te} = \pi k\frac{\sqrt{r_0^2 + c_2^2 - a^2} - r_0}{r_0}(r_0^2 + c_2^2 - a^2). \tag{11}$$

The adhesive energy is defined:

$$U_{ad} = \gamma_{12}\pi b^2. \tag{12}$$

Insert 3, 11, 12 into (1), we have:

$$U_{tot} = \int Fdz = pV_1 - p\frac{\pi}{6}c_2\left(3r_0^2 + c_2^2\right) + p\frac{\pi}{6}a\left(3b^2 + a^2\right)$$
$$+\pi k\frac{\left(r_0^2 + c_2^2 - a^2\right)^{\frac{3}{2}}}{r_0} - \pi k\left(r_0^2 + c_2^2 - a^2\right) - \gamma_{12}\pi b^2. \tag{13}$$

Equilibrium state will obtain when

$$\frac{dU_{tot}}{db} = 0 \rightarrow \frac{dU_{tot}}{db} = \frac{dU_{tot}}{db} + \frac{dU_{tot}}{dz}\frac{dz}{db} = 0, \tag{14}$$

with z is a function over c_2 and a: $z = c_1 - c_2 + a$.

The pressing force is the derivation of total energy over a variant of displacement following the z-axis.

$$\frac{dU_{tot}}{dz} = F,$$
$$\frac{dz}{db} = \frac{d(c_1 - c_2 + a)}{db} = \frac{da}{db},$$
$$a = R_2 - \sqrt{R_2^2 - b^2}. \tag{15}$$

The result of derivation leads to the equation as below:

$$\pi\left(pR_2 - p\sqrt{R_2^2 - b^2} - 2\gamma_{12}\right)\sqrt{R_2^2 - b^2} - F = 0.$$

Because $a << R_2, b << R_2$, we have $\sqrt{R_2^2 - b^2} \approx R_2$

$$\longrightarrow b = \sqrt{\frac{F + 2\gamma_{12}\pi\left(\frac{r_0^2 + c_2^2}{2c_2}\right)}{p\pi}}. \tag{16}$$

We consider the force that presses into the surface at the equilibrium of state 2.

$$F = \frac{dU_{tot}}{dz} = \frac{dU_{tot}}{da}\frac{dU_a}{dz} + \frac{dU_{tot}}{dc_2}\frac{dc_2}{dz} + \frac{dU_{tot}}{db}\frac{db}{dz}.$$

By the condition of (14) and (15)

$$\longrightarrow F = \frac{p\pi}{2}\left(b^2 + a^2 + r_0^2 + c_2^2\right)$$
$$-\frac{3k\pi}{r_0}(c_2 + a)\sqrt{r_0^2 + c_2^2 - a^2} + 2k\pi(a + c_2). \tag{17}$$

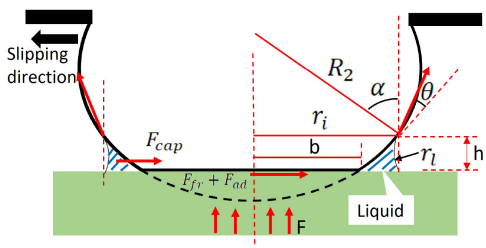

Fig. 4. Capillary action upon contact with the wet floor, generated by a liquid layer surrounding the soft pad with height h. In this case, the pad tends to slip to the left.

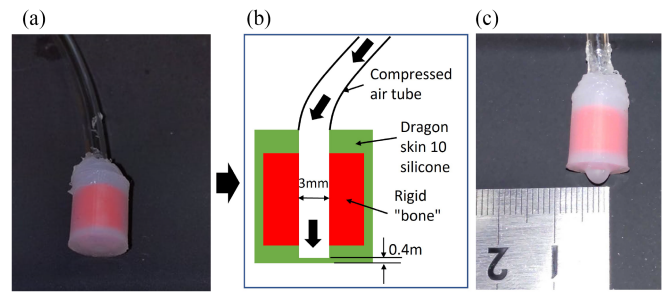

Fig. 5. Soft pad design. (a) Soft pad without air pressure. (b) Concept of soft pad design. (c) Soft pad with air pressure.

Here, we found a homogeneous constrain as follows:

$$\frac{r_0^2+c_2^2}{2c_2}=\frac{a^2+b^2}{2a}. \tag{18}$$

When $F=0 \longrightarrow a=0, b=0$, equation (17) and (18) become:

$$F=\frac{p\pi}{2}\left(r_0^2+c^2\right)-\frac{3k\pi}{r_0}(c+a)\sqrt{r_0^2+c^2}+2k\pi\ (a+c), \tag{19}$$

$$\frac{r_0^2+c^2}{2c}=\frac{a^2+b^2}{2a}. \tag{20}$$

The root of the system of equations (20), (21) is the geometrical parameter c_1 of step 1. Then we have $R_1=\frac{r_0^2+c_1^2}{2c_1}$. The root of the system of equations (17)–(19) is the geometrical parameter of step 2 that includes c_2, a, b, and then we have $R_2=\frac{r_0^2+c_2^2}{2c_2}$. The roots of the system of the equation are solved by the numerical method *vpasolve* of MATLAB.

B. Contact Model With Liquid Film

In the previous section, the specifications of a soft pad in spherical dome status for one cycle were calculated based on contact force F and inner pressure p. Here, we assume that the dome came into contact with the surface through a liquid film as illustrated in Fig. 4. Under surface tension, capillary action occurs around the periphery of the soft pad contact area in the presence of a liquid. We attempt to model the resultant resistive force acting on the contact interface with capillary action to demonstrate the role of the dome in enhancement of locomotion. Here, tangential resistive force is calculated as:

$$F_{re}=F_{fr}+F_{ad}+F_{cap}, \tag{21}$$

where:

$$F_{fr}=\mu N, F_{ad}=\tau A. \tag{22}$$

Let us consider the role of capillary action in the total tangential resistive force. The pressure difference in the liquid creates resistance when the spherical pad tends to move, that called the tangential capillary force. Therefore, the tangential capillary force can be estimated as follows:

$$F_{cap}=\int_S \Delta p_l dS\cos\phi \rightarrow F_{cap}=\Delta p_l h 2r_i, \tag{23}$$

$$\Delta p_l=\gamma_l\left(-\frac{1}{r_l}-\frac{1}{r_i}\right), \text{and } h\approx 2r_l,\ F_{cap}=-2\gamma_l\left(2r_i+h\right). \tag{24}$$

Applying Newton's laws to the system of force for wet adhesion and the weight of amount of wetted liquid, we obtain:

$$\rho g V_l=2\pi\gamma_s\sin(\theta+\alpha), \tag{25}$$

$$\rightarrow \frac{h\rho g}{3}\left[b+2h\cot\alpha-\frac{b}{(b+h\cot\alpha)}b\right]=2\gamma_s\sin(\theta+\alpha), \tag{26}$$

$$\text{with } \frac{b}{(b+h\cot\alpha)}\approx 1,$$

$$\text{and } h=\sqrt{\frac{3\gamma_s\sin(\theta+\alpha)}{\rho g\cot\alpha}}, \cos\theta=\left(2\sqrt{\frac{\gamma_s}{\gamma_l}}-1\right).$$

Insert these values into (23), resulting in the simplified estimation of F_{cap} as follows:

$$F_{cap}=-2\gamma_l\left[2b+(2\cot\alpha+1)\sqrt{\frac{3\gamma_s\sin(\theta+\alpha)}{\rho g\cot\alpha}}\right]. \tag{27}$$

Consequently, we constructed a model to explain air pressure induced change in spherical pad morphology. Then, we showed the advantage of enhancing tangential force by morphology computation.

IV. Experiment

To evaluate estimations in the previous section, we conducted experiments using a soft pad (spherical dome) (see Fig. 5), whose morphology can be changed by varying the air pressure. The red rigid bone (3-D printed) enveloped by a silicone skin layer (Dragon skin 10, Smooth-On, Inc., USA) houses a cylindrical chamber (3 mm dia.) channeling compressed air to inflate a soft pad (initial thickness 0.4 mm). The radius r_0 was initially designed to maximize the number of contact pairs between soft sphere pads and the road (i.e., increase contact area as well as the impact of the capillary phenomenon) while still satisfying the fabrication capability.

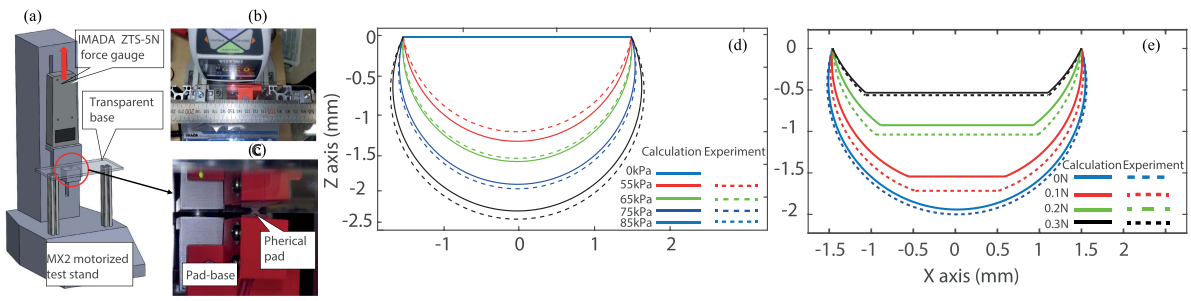

Fig. 6. Design of experiment state 2. (a) Setup to test morphology change. (b) Soft pad pressure measurement. (c) Practical pressed soft pad. (d) Experiment state 1: Effects of different pressures in the soft pad without floor contact were compared using Matlab. (e) Experiment state 2: Response of the soft pad under air pressure of 75 kPa to being pressed at different forces.

A. Inflation and Contact-Related Shape Verification

In the first experiments, air pressure was set to 55 kPa, 65 kPa, 75 kPa, or 85 kPa (by using the external air compressor) and the dome shape of the inflated pad was measured. The elasticity coefficient was measured as 40 N/m using an MX2 Motorized test stand. In fact, the elasticity coefficient may vary according to Young's modulus under different states of deformation, especially under large deformation. However, in this case, we considered the soft pad dome deformation to be in the linear area of the Young's modulus giving a constant elasticity coefficient. Besides, the relative surface energy between silicone and acrylic in this experiment $\gamma_{12} = 2\sqrt{\gamma_1\gamma_2}$ is 0.006 J/m^2 [26]. In this experiment, the resultant shape of the inflated dome was measured as Fig. 6(a), (b), (c), wherein we measured the values of $b, r_0, d = (c_2 - a)$ (see Fig. 2(d)). The radius and height of the dome was calculated as $c_2 = \frac{\sqrt{(r_0^2-b^2-d^2)^2+4r_0^2 d^2}-(r_0^2-b^2-d^2)}{2d}$, and $R_2 = \frac{(r_0^2+c_2^2)}{2c_2}$

Then, the results of the experiment were plotted in (Fig. 6(d)) in comparison with calculated values using the method described in the previous section. The errors were around $\pm 3\%$. As the result given in Fig. 6(d), (e), the error tended to rise with air pressure. This trend was caused by change in elasticity coefficient k that increased with deformation.

In the contact experiment, the air pressure was kept at 75 kPa and the soft pad dome was pressed against a rigid surface. Fig. 6(a) shows the system setup, where the soft pad is affixed to a force gauge (IMADA ZTS-5 N) which may be vertically translated by a motor. The contact area of the soft pad dome was observed through a transparent base, and the shape of the contacting dome pad was determined. In trials, the press force was set at 0.1 N, 0.2 N, or 0.3 N, respectively. Experiment and calculation results are shown in Fig. 6(e). Error between the calculated and experimental results decreased at compression forces 0.1 N, 0.2 N, and 0.3 N, respectively. This is because when compression force increased deformation decreased in turn, increasing elasticity coefficient k towards the calculation value.

B. Tangential Force Experiment

In this section, we evaluate the role of capillary action on the soft pad dome in resistance to slippage. The experimental apparatus is shown in Fig. 7(a), which includes two motorized linear stages for vertical and horizontal movements. The experiment was conducted under wet and dry conditions, with the soft pad morphology ranging from flat to domed at 65 kPa, 75 kPa, and 85 kPa, respectively. The resultant capillary force F_{cap} was assumed to be the difference between F_{wet} and F_{dry}, which are the tangential forces measured in each condition, respectively, i.e. $F_{cap} = F_{wet} - F_{dry}$. Then, the measured tangential forces when the soft pad was in the domed shape were compared with those when it was flat (in both dry and wet scenarios). Note that tangential force was recorded *before* total slippage of the contact surface, which is referred to as incipient slip (see [27]). A test trial commenced by pressing the soft pad onto a surface fixed on a 3-axis force sensor (DSS300-U, TecGihan, Japan) at different values of contact force. Then, the horizontal linear stage was activated to exert tangential displacement of the soft pad at a speed of 0.2 mm/s, which was small enough to avoid any effect of viscosity. Obtained results are summarized in Fig. 8.

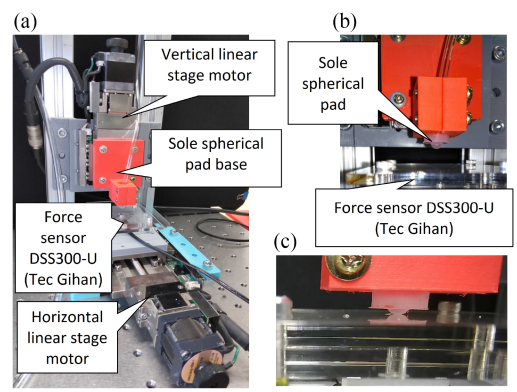

Fig. 7. Experiment to test soft pad resistance to tangential force. (a) Experimental setup. (b) Soft pad under air pressure without simulated floor contact, (c) and with simulated wet floor contact.

Under the dry condition, a flat soft pad (i.e., without spherical dome induced air pressure) showed greatest tangential forces w.r.t a range of normal forces (up to 0.4 N). However, under the wet condition the resultant tangential force acting on the soft pad with a flat surface was reduced by 1.5-2 fold. This result demonstrated that a flat soft pad morphology was only suitable for dry environments, since in the wet condition this

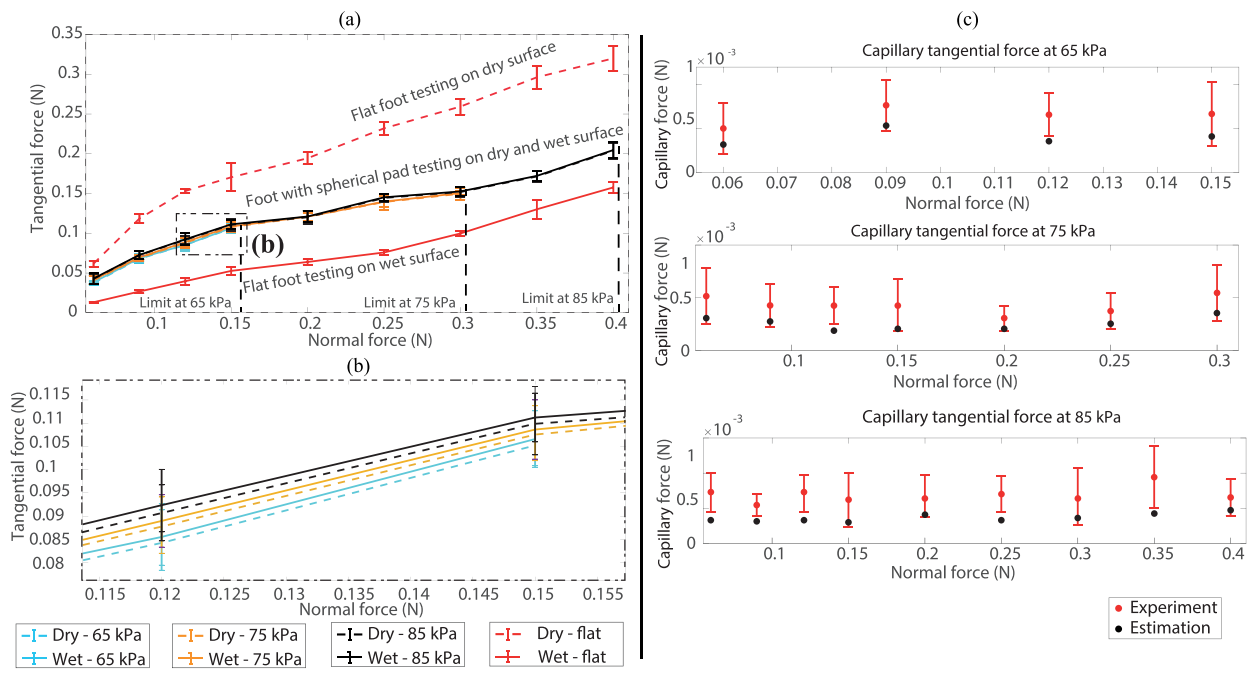

Fig. 8. (a) Comparison of resulted tangential forces among flat soft pad, and domed pad under pressures of 65 kPa, 75 kPa, and 85 kPa, respectively; on both wet and dry floors. (b) Zoom-in range with comparison of tangential forces under dry (dashed line) and wet (solid line) conditions several air pressure values. (c) Comparison of capillary action in wet condition ($F_{cap} = F_{wet} - F_{dry}$) between experiment (with error bars) and estimation results.

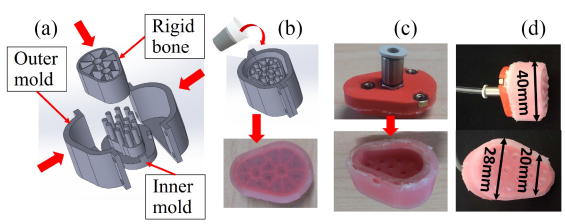

Fig. 9. Fabrication process: (a) mold set of foot. (b) Pouring silicone. (c) Finishing the foot. (d) soft pad under pressurization and dimension.

shape pad might slip due to low tangential force. For the domed soft pad morphology, we set movement of the contact pad at a low speed of 0.2 mm/s to ensure slippage would not occur. Also, the air pressure was varied to examine morphological impact. Fig. 8(a), (b) reveal slight differences in tangential force values between the two conditions: wet (solid lines) and dry (broken lines). More importantly, tangential force associated with the domed soft pad was higher than that with the flat pad in the wet condition, suggesting better walking stability of a domed than a flat soft pad. Accordingly, we conclude that a *flat soft pad is suitable for walking on a dry surface and a domed one for walking on a wet surface*. Regarding a domed soft pad, and the effect of its morphology (represented by inner pressure) on resultant tangential force. When the soft pad is pressed onto the contact surface, the dome cannot endure high normal force, since it may surpass the potential energy of the inner pressure. Thus, at each morphological state of the dome, there exists a limit of normal force. Based on our measurements, the limits of normal force at 65 kPa, 75 kPa, and 85 kPa are 0.15 N, 0.3 N, and 0.4 N, respectively (as indicated in the horizontal axis of Fig. 9(a)). As revealed by the proposed analytical model (see (17)–(19)), lower normal force results in reducing the tangential force generated during the contact phase. Therefore, increasing the air pressure to change the morphology is necessary to increase the normal force limit, thus enhancing the tangential force. Besides, the silicone Dragon skin 10 (Shore Hardness 10 A) can be changed to Dragon skin 20 (Shore Hardness 20 A), or Dragon skin 30 (Shore Hardness 30 A) to increase the limit of normal force. In Fig. 8(c), we compare the resultant capillary force F_{cap} of a domed pad in wet condition, w.r.t. three levels of air pressure (65 kPa, 75 kPa, and 85 kPa) with the estimated value using the proposed analytical model (see (28)). Although the complication of liquid film at the contact area increased capillary action in the experiment bringing errors of 10%–26%, the trend of the experiment results meets the estimation.

V. Showcase: Walking Leg

A. Design and Fabrication

In this section, we showcase walking efficiency on each of a wet and a dry surface of a leg with a foot that includes either a flat or a domed soft pad. For simplicity, the walking system includes only one leg, however, the results are promising to verify the applicability of this device into other complex systems in the future. The foot design is shown in Fig. 9(c), (d), including an inner "bone" (in red, 3D-printed), covered by a membrane of silicone skin. The bottom layer (sole) contains a set of spherical domes arranged as in Fig. 9(b). The rigid bone is connected to an external air-pressure regulator through a hose. Initially, the sole of the foot is in a flat state (see Fig. 9(d)). When energized by air pressure, soft pad domes emerged from the sole. The process of fabrication is shown in Fig. 9(a)–(c): the silicone is filled

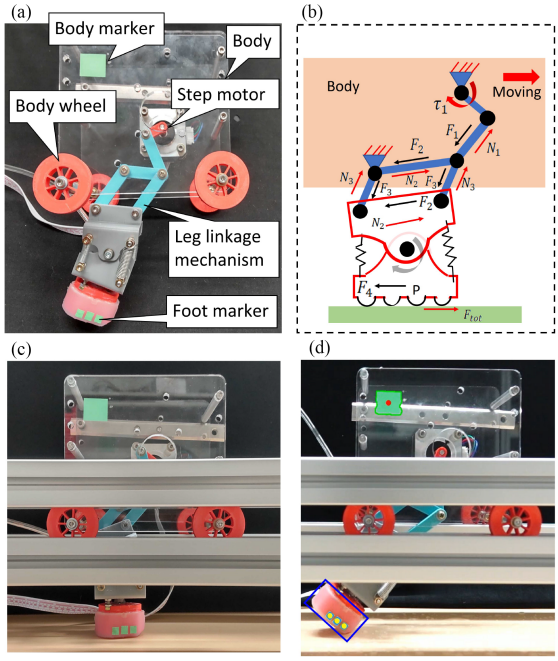

Fig. 10. Design of the robotic leg. (a) The walking system with constituted parts. (b) Mechanical analysis of the linkage system for walking tests on (c) dry, and (d) wet floors (tracked contour data was used to plot the paths of the foot in Fig. 11).

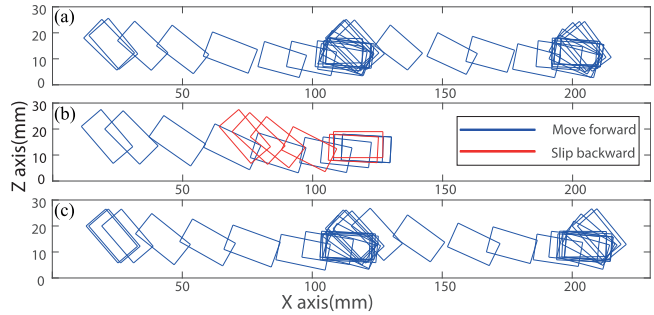

Fig. 11. Tracked foot's posture (the rectangle in Fig. 10(d) during walking action in (a) on a dry floor, (b) on a wet floor with flat foot, and (c) on a wet floor with domed pad (high inner pressure state).

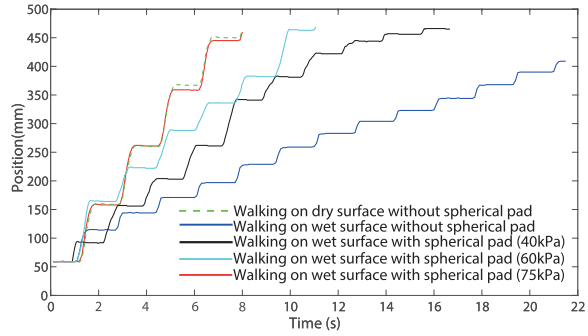

Fig. 12. Results of the walking robot's body displacement in five experimental conditions (tracked by the marker on the robot body as shown in Fig. 12(d)).

in the outer mold to cover the rigid bone and shape the foot. Besides, the inner mold would form air hoses for directing air for inflating the thin sheet in the container. The 3D-printed cap is used to assemble with the molded product for the completed foot.

B. Showcase Experiment of Walking Leg

The walking mechanism includes a body that carries a step motor to actuate a one-dof (degree of freedom) linkage system (see Fig. 10(a)). To evaluate efficiency in prevention of foot slippage, the walking mechanism was kept simple to avoid artifacts caused by a complicated walking system. Here, we tested the one-leg mechanism moving on four wheels constrained by a rail system (see Fig. 10(c), (d)). The concept of the linkage mechanism is showed in Fig. 10(b), in which the torque τ_1 of the step motor makes external forces F_1, F_2, F_3, F_4. The hinge joint between the foot and the linkage system supported by two springs is for pressing the foot to the floor, while increasing the contact time between the foot and the floor. The external force F_4 makes the foot tend to move backward. In the case that the tangential resistance force F_{tot} is sufficient, slippage between the foot and surface would not occur, and the foot is still until reactive forces N_1, N_2, N_3 push the body moving forward. Motion of the walking body was tracked via a green marker (body marker); and three smaller markers attached to the foot to extract stick/slip motion of the foot upon walking. A camera (SONY RX10IV(DSC-RX10M4) was set facing the walking system to capture movement of markers (see Fig. 10(c), (d). Two dimensional movement of markers were extracted using OpenCV [28]. By detecting the contour of the foot based on movement of the markers, we evaluated walking efficiency in five walking cases: 1, on a dry surface (flat soft pad); 2, on a wet surface (flat soft pad); 3–5, on a wet surface with a domed soft pad pressurized at 40 kPa, 60 kPa, or 75 kPa, respectively. For the first case, foot posture during walking phases is plotted in Fig. 11(a), wherein it comes into contact with the surface firmly (without slippage), pushes the body moving forward before stably lifting off from the surface. For the second case, foot posture is recorded in Fig. 11(b). The foot with a flat soft pad failed to walk well in the wet condition. The foot came into contact with the wet surface (represented by blue rectangles) then, due to low resultant tangential force, instead of pushing the body forward, it started to slip backward (represented by red rectangles). This result supports the experimental observation in the previous section, in which the wet condition significantly reduces the tangential force of the flat pad. For the third case, walking on the wet surface with a domed soft pad, locomotion of the foot was similar to that of case 1 (a flat soft padded foot walking on a dry surface), in which there was almost no slippage upon landing of the foot (see the plot in Fig. 11(c)). This result clearly showcases the potential of the domed soft pad in improving walking efficiency in a wet environment.

Finally, we summarize time-series positions of the robot body in all five cases in Fig. 12. Notably, movements of the body in case 1 (flat pad, dry surface) and case 5 (domed pad, wet surface, 75 kPa) were similar. The foot performed fast

walking without notable slippage, and reached the destination successfully. In contrast, reaching the goal by case 2 (flat pad, wet surface) took approximately five times longer than case 5, requiring many more walking cycles due to slippage. Varying the domed pad morphology with air pressure (at 40 kPa and 60 kPa, respectively), showed that higher pressure improved walking performance. In a flat state, or domed state with low air pressure, a layer of liquid was trapped between the foot and the contact surface changing dry friction-adhesion into lubrication decreasing tangential resistance force leading to slippage. In contrast, with sufficient air pressure the liquid was expelled from the contact interface to maintain dry friction-adhesion upon contact. In addition, the liquid layer was swept randomly on a large area, and we could not ensure that the liquid layer surrounding the soft pad was equally distributed around the domes. In fact, it was not our purpose in this experiment, since in the practical case of walking, it is difficult to secure the said condition of liquid layer. Thus, the capillary force in the walking leg experiment (even practical walking of robots) is smaller than we expect in the analytical model. Regardless, the uneven height of the liquid still causes the capillary force (although smaller than the capillary estimated in the model) that plays a role in the tangential capillary, and helps the robot improve walking on wet surfaces.

VI. Conclusion

The role of capillary action in tangential resistance force was demonstrated by analytical modeling and experiments. The morphology-changeable soft pad should be kept flat when walking on dry floor, while must be transformed to domed shapes for enhancing the walking efficiency in wet environment. The results provide a foundation for the study of tribology that explain the phenomena of animal locomotion that may be applied to the design of a legged walking robot. Future work is intended: 1) experiments towards developing a walking robot, 2) investigations into the relation between deformation and tangential resistance force coefficient, 3) and the distribution of soft pads may affect tangential resistance force.

Acknowledgment

The authors would like to thank Mr. Linh Viet Nguyen and Mr. Nhat Dinh Minh Le (Soft Haptics Lab., School of Materials Science, Japan Advanced Institute of Science and Technology) for their valuable help in conducting experiments.

References

[1] J. Hwang, Y. Jeong, J. M. Park, K. H. Lee, J. W. Hong, and J. Choi, "Biomimetics: Forecasting the future of science, engineering, and medicine," *Int. J. Nanomedicine*, vol. 10, 2015, Art. no. 5701.

[2] S. Kim, C. Laschi, and B. Trimmer, "Soft robotics: A bioinspired evolution in robotics," *Trends Biotechnol.*, vol. 31, no. 5, pp. 287–294, 2013.

[3] J. E. Bernth, V. A. Ho, and H. Liu, "Morphological computation in haptic sensation and interaction: From nature to robotics," *Adv. Robot.*, vol. 32, no. 7, pp. 340–362, 2018, doi: 10.1080/01691864.2018.1447393.

[4] V. C. Müller and M. Hoffmann, "What is morphological computation? on how the body contributes to cognition and control," *Artif. Life*, vol. 23, no. 1, pp. 1–24, 2017.

[5] S. Singla et al., "Direct evidence of acid-base interactions in gecko adhesion," *Sci. Adv.*, vol. 7, no. 21, 2021, Art. no. eabd9410.

[6] F. Meng, Q. Liu, X. Wang, D. Tan, L. Xue, and W. J. P. Barnes, "Tree frog adhesion biomimetics: Opportunities for the development of new, smart adhesives that adhere under wet conditions," *Philos. Trans. Roy. Soc. A*, vol. 377, no. 2150, 2019, Art. no. 20190131.

[7] R. D. Prusch, "Solute secretion by the tube foot epithelium in the starfish Asterias forbesi," *J. Exp. Biol.*, vol. 68, no. 1, pp. 35–43, 1977.

[8] M. Algrain, E. Hennebert, P. Bertemes, R. Wattiez, P. Flammang, and B. Lengerer, "In the footsteps of sea stars: Deciphering the catalogue of proteins involved in underwater temporary adhesion," *Open Biol.*, vol. 12, no. 8, 2022, Art. no. 220103.

[9] G. Hanna, W. Jon, and W. J. Barnes, "Adhesion and detachment of the toe pads of tree frogs," *J. Exp. Biol.*, vol. 155, no. 1, pp. 103–125, 1991.

[10] J. K. Langowski, D. Dodou, M. Kamperman, and J. L. van Leeuwen, "Tree frog attachment: Mechanisms, challenges, and perspectives," *Front. Zool.*, vol. 15, no. 1, pp. 1–21, 2018.

[11] K. Autumn, "How gecko toes stick: The powerful fantastic adhesive used by geckos is made of nanoscale hairs that engage tiny forces, inspiring envy among human imitators," *Amer. Scientist*, vol. 94, no. 2, pp. 124–133, 2006.

[12] J. Yu et al., "Gecko-inspired dry adhesive for robotic applications," *Adv. Funct. Mater.*, vol. 21, no. 16, pp. 3010–3018, 2011.

[13] G. Huber et al., "Evidence for capillarity contributions to gecko adhesion from single spatula nanomechanical measurements," *Proc. Nat. Acad. Sci.*, vol. 102, no. 45, pp. 16293–16296, 2005.

[14] R. Santos, S. Gorb, V. Jamar, and P. Flammang, "Adhesion of echinoderm tube feet to rough surfaces," *J. Exp. Biol.*, vol. 208, no. 13, pp. 2555–2567, 2005.

[15] M. A. Bell et al., "Echinoderm-inspired tube feet for robust robot locomotion and adhesion," *IEEE Robot. Automat. Lett.*, vol. 3, no. 3, pp. 2222–2228, Jul. 2018.

[16] A. Ji, Z. Zhao, P. Manoonpong, W. Wang, G. Chen, and Z. Dai, "A bio-inspired climbing robot with flexible pads and claws," *J. Bionic Eng.*, vol. 15, no. 2, pp. 368–378, 2018.

[17] Y. Chen, N. Doshi, and R. J. Wood, "Inverted and inclined climbing using capillary adhesion in a quadrupedal insect-scale robot," *IEEE Robot. Automat. Lett.*, vol. 5, no. 3, pp. 4820–4827, Jul. 2020.

[18] K. L. Johnson, K. Kendall, and A. Roberts, "Surface energy and the contact of elastic solids," *Proc. Roy. Soc. London. A. Math. Phys. Sci.*, vol. 324, no. 1558, pp. 301–313, 1971.

[19] B. V. Derjaguin, V. M. Muller, and Y. P. Toporov, "Effect of contact deformations on the adhesion of particles," *J. Colloid Interface Sci.*, vol. 53, no. 2, pp. 314–326, 1975.

[20] K. Fuller and D. Tabor, "The effect of surface roughness on the adhesion of elastic solids," *Proc. Roy. Soc. London. A. Math. Phys. Sci.*, vol. 345, no. 1642, pp. 327–342, 1975.

[21] D. Maugis, "Adhesion of spheres: The JKR-DMT transition using a dugdale model," *J. Colloid Interface Sci.*, vol. 150, no. 1, pp. 243–269, 1992.

[22] P. Van Nguyen and V. A. Ho, "Mechanics of wet adhesion in soft interaction with patterned morphology," *Bioinspiration Biomimetics*, vol. 14, no. 1, 2018, Art. no. 016005.

[23] P. V. Nguyen and V. A. Ho, "Grasping interface with wet adhesion and patterned morphology: Case of thin shell," *IEEE Robot. Automat. Lett.*, vol. 4, no. 2, pp. 792–799, Apr. 2019.

[24] P. Van Nguyen and V. A. Ho, "Wet adhesion of soft curved interfaces with micro pattern," *IEEE Robot. Automat. Lett.*, vol. 6, no. 3, pp. 4273–4280, Jul. 2021.

[25] W. A. Osborne and W. Sutherland, "The elasticity of rubber balloons and hollow viscera," *Proc. Roy. Soc. London. Ser. B., Containing Papers Biol. Character*, vol. 81, no. 551, pp. 485–499, 1909.

[26] V. L. Popov, *Contact Mechanics and Friction*. Berlin, Germany: Springer, 2010.

[27] V. A. Ho and S. Hirai, "Understanding slip perception of soft fingertips by modeling and simulating stick-slip phenomenon," in *Robotics: Science and System VII*. Cambridge, MA, USA: MIT Press, 2012, pp. 129–136.

[28] G. Bradski, "The OpenCV library," *Dr. Dobb's J. Softw. Tools Professional Programmer*, vol. 25, pp. 120–123, 2000.